Drill-string nonlinear dynamics accounting for the drilling fluid

T.G. Ritto, R. Sampaio, Christian Soize

DRILL-STRING NONLINEAR DYNAMICS ACCOUNTING FOR DRILLING FLUID

T. G. Ritto
R. Sampaio
thiagoritto@gmail.com
rsampaio@puc-rio.br
PUC-Rio, Rua Marquês de São Vicente 225, 22453-900, RJ, Brasil
C. Soize
christian.soize@univ-paris-est.fr
Université Paris-Est, Laboratoire de Modélisation et Simulation Multi Echelle,
MSME FRE3160 CNRS, 5 bd Descartes, 77454 Marne-la-Vallée, France

Abstract. *The influence of the drilling fluid (or mud) on the drill-string dynamics is analyzed in this paper. Usually the presence of the fluid is not taken into account in the analysis of the nonlinear dynamics of a drill-string. The aim of this paper is to investigate how the fluid affects this dynamics using a simplified fluid-structure interaction model that takes into account the fluid that flows downward inside the column and then upward in the annulus. For the column, the proposed model considers the Timoshenko beam theory with finite strain (all the terms of the Green-Lagrange tensor are used). When finite strains are considered, the axial, lateral and torsional vibrations become coupled. A bit-rock interaction model that describes how the bit penetrates the soil is used and there might be impact and rubbing between the column and the borehole. The system of equations is discretized by mean of the Finite Element Method. It turns out that the fluid has an important influence on the drill-string dynamics, especially for the lateral vibrations.*

Keywords: *drill-string dynamics, nonlinear dynamics, fluid-structure interaction*

1. INTRODUCTION

A drill-string is a slender structure used in oil wells to penetrate the soil in search of oil. There are still many challenges involving the modeling of this complex dynamics that involves bit-rock interaction, fluid-structure interaction, coupling vibrations and also impact. There are many papers that analyze the nonlinear dynamics of a drill-string, *e.g.* Tucker and Wang (1999); Christoforou and Yigit (2003); Trindade et al. (2005); Richard et al. (2007); Khulief et al. (2007), however, none of these works consider the fluid-structure interaction. In references Tucker and Wang (1999); Christoforou and Yigit (2003) the influence of the fluid is considered in a simplistic way.

Fig. 1 shows a sketch of a drill-string. The upper region is composed by thin tubes called drill-pipes and the bottom region, called Bottom-Hole-Assembly (BHA), is composed by thicker tubes called drill-collars.

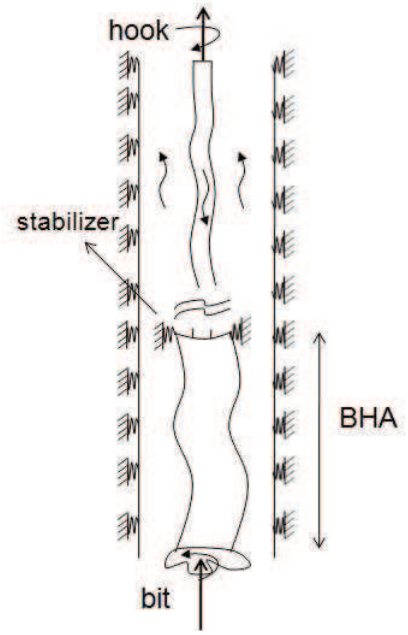

Figure 1: Sketch of a drill-string.

The drilling fluid (mud) is responsible to transport the cuttings (drilled solids) from the bottom to the top to avoid clogging of the hole. The fluid flows downward inside the column and then upward in the annulus. It also plays an important role in cooling the bit and stabilizing the system (ASME, 2005). The mud has complex rheological properties, see for instance Coussot et al. (2004). There is no doubt that the drilling fluid influences the dynamics of a drill-string, but to solve the complete problem would be too expensive computationally. There are some works that study only the drilling-fluid flow, as, for example, Escudier et al. (2000, 2002); Pina and Carvalho (2006).

The aim of this paper is to investigate how the presence of the drilling fluid influences the dynamics of a drill-string. For doing so, a simple model that considers the fluid that flows downward inside the column and then upward in the annulus is presented. This model is an extension of the one developed in Paidoussis et al. (2008) and it permits the influence of the fluid to be computed by adding an axial force and a mass, a damping and a stiffness matrix that are constant on time.

Besides the inclusion of the fluid in the nonlinear dynamics of the drill-string, the proposed

model has a new feature which is the use of the Timoshenko beam theory with finite strain (using all the terms of the Green-Lagrange strain). The equations of motions are derived using the extended Hamilton Principle and then they are discretized by means of the Finite Element Method.

The paper is organized as follows. In Section 2. the model is presented, it includes finite strain, impact and the bit-rock interaction. In Section 3. the fluid-structure interaction model is depicted in details. In Section 4. the final discretized system of equations are presented. Then, the numerical results are discussed in Section 5. and the conclusions are made in Section 6..

2. MODEL

In this section the standard model without the fluid-structure interaction is described. The fluid-structure interaction model is discussed in section 3..

Previous papers Christoforou and Yigit (2003); Trindade et al. (2005); Khulief et al. (2007) have used the Euler-Bernoulli beam theory (which neglects shear) to model the drill-string. In this work the Timoshenko beam theory (which considers shear) is used because (1) it includes the Euler-Bernoulli theory and (2) it allows us to inquire about the importance of shear in the dynamics of this nonlinear system. A 3D beam model is used with six degrees of freedom in each interpolation point: the three translational displacements of the neutral line (axial u, lateral in y-axis v and lateral in z-axis w) and the three rotations of the cross sections (about the x-axis θ_x, about the y-axis θ_y and about the z-axis θ_z). It is assumed small angles for θ_y and θ_z, which is justified because the vibration of the column is constrained inside the borehole, however θ_x is finite.

The equations of motion are derived using the extended Hamilton Principle for which the first variation of the potential Π must vanish:

$$\delta\Pi = \int_{t_1}^{t_2} (\delta U - \delta T - \delta W) dt = 0\,, \tag{1}$$

where U is the potential strain energy, T is the kinetic energy and W is the work done by the nonconservative forces and by any force not accounted in the potential energy.

The system is discretized using the Finite Element Method. The element displacements and rotations are written as $u^e(x,t) = \mathbf{N}_u(x)\mathbf{u}^e(t)$, $v^e(x,t) = \mathbf{N}_v(x)\mathbf{u}^e(t)$, $w^e(x,t) = \mathbf{N}_w(x)\mathbf{u}^e(t)$, ${\theta_x}^e(x,t) = \mathbf{N}_{\theta_x}(x)\ \mathbf{u}^e(t)$, ${\theta_y}^e(x,t) = \mathbf{N}_{\theta_y}(x)\mathbf{u}^e(t)$, ${\theta_z}^e(x,t) = \mathbf{N}_{\theta_z}(x)\mathbf{u}^e(t)$, where $\mathbf{N}$ are the shape functions (see appendix A) and $\mathbf{u}^e = \begin{pmatrix} u_1 & v_1 & \theta_{z1} & w_1 & \theta_{y1} & \theta_{x1} & u_2 & v_2 & \theta_{z2} & w_2 & \theta_{y2} & \theta_{x2} \end{pmatrix}^T$, $(\cdot)^T$ denotes transpose. Fig. 2 shows the two node finite element used in the numerical model (l^e is the length of the element).

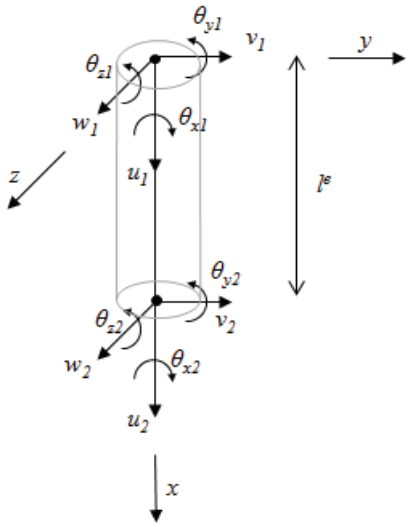

Figure 2: Two node finite element with six degrees of freedom per node.

2.1 Kinetic energy

The kinetic energy is written as

$$T = \frac{1}{2}\int_0^L \rho(A\mathbf{v}^T\mathbf{v} + \mathbf{w}^T\mathbf{I}\mathbf{w})\,dx\,, \tag{2}$$

where ρ is the mass density, A is the cross-sectional area, L is the length of the column, $\mathbf{v}$ is the velocity vector, $\mathbf{I}$ is the cross-sectional inertia matrix and $\mathbf{w}$ is the section angular velocity vector:

$$\mathbf{v} = \begin{bmatrix} \dot{u} \\ \dot{v} \\ \dot{w} \end{bmatrix}\,,\ \mathbf{I} = \begin{bmatrix} I_p & 0 & 0 \\ 0 & I & 0 \\ 0 & 0 & I \end{bmatrix}\,,\ \mathbf{w} = \begin{bmatrix} \dot{\theta}_x + \theta_y\dot{\theta}_z \\ \cos(\theta_x)\dot{\theta}_y - \sin(\theta_x)\dot{\theta}_z \\ \sin(\theta_x)\dot{\theta}_y + \cos(\theta_x)\dot{\theta}_z \end{bmatrix}\,. \tag{3}$$

The time derivative (d/dt) is denoted by a superposed dot. In Eq. (3) I is the cross-sectional moment of inertia and I_p is the polar moment of inertia. The angular velocity vector $\mathbf{w}$ is written in the inertial frame and it is derived by first rotating the inertial frame about the x-axis θ_x, then rotating the resulting frame about the y-axis θ_y and, finally, rotating the resulting frame about the z-axis θ_z. This was done under the hypothesis of small angles θ_y and θ_z.

Note that the rotational speed about the x-axis $\dot{\theta}_x$ is not constant, therefore the discretization of kinetic energy yields a constant mass matrix $\mathbf{M}$ and a nonlinear force vector $\mathbf{f}_{ke}$ that couples axial, torsional and lateral vibrations. The mass element matrix is written as:

$$\begin{aligned}\mathbf{M}^e = \int_0^1 &[\rho A(\mathbf{N}_u^T\mathbf{N}_u + \mathbf{N}_v^T\mathbf{N}_v + \mathbf{N}_w^T\mathbf{N}_w) + \\ &+\rho I(\mathbf{N}_{\theta_y}^T\mathbf{N}_{\theta_y} + \mathbf{N}_{\theta_z}^T\mathbf{N}_{\theta_z}) + \rho I_p(\mathbf{N}_{\theta_x}^T\mathbf{N}_{\theta_x})]\; l^e d\xi\,.\end{aligned} \tag{4}$$

where ξ is the element coordinate ($\xi = x/l^e$). Using the rotational speeds $\dot{\theta}_x^e = \mathbf{N}_{\theta_x}\dot{\mathbf{u}}^e$, $\dot{\theta}_y^e = \mathbf{N}_{\theta_y}\dot{\mathbf{u}}^e$, $\dot{\theta}_z^e = \mathbf{N}_{\theta_z}\dot{\mathbf{u}}^e$ and the angular accelerations $\ddot{\theta}_x^e = \mathbf{N}_{\theta_x}\ddot{\mathbf{u}}^e$, $\ddot{\theta}_y^e = \mathbf{N}_{\theta_y}\ddot{\mathbf{u}}^e$, $\ddot{\theta}_z^e = \mathbf{N}_{\theta_z}\ddot{\mathbf{u}}^e$, the nonlinear force element vector due to the kinetic energy is written as:

$$(\mathbf{f}^{ke})^{(e)} = \rho I_p \int_0^1 \left[\mathbf{N}_{\theta_x}^T (\theta_y^e \ddot{\theta}_z^e + \dot{\theta}_y^e \dot{\theta}_z^e) + \mathbf{N}_{\theta_z}^T (\theta_y^e \ddot{\theta}_x^e + \dot{\theta}_y^e \dot{\theta}_x^e) - \mathbf{N}_{\theta_y}^T (\dot{\theta}_x^e \dot{\theta}_z^e) \right] l^e d\xi \,. \tag{5}$$

2.2 Strain energy

The strain energy is written as:

$$U = \frac{1}{2} \int_V \boldsymbol{\epsilon}^T \mathbf{S} dV \,, \tag{6}$$

where V is the volume, $\boldsymbol{\epsilon}$ is the Green-Lagrange strain tensor and $\mathbf{S}$ is the second Piola-Kirchhoff stress tensor (written in Voigt notation). The stress-strain relationship is given by $\mathbf{S} = \mathbf{D}\boldsymbol{\epsilon}$:

$$\begin{bmatrix} \sigma_{xx} \\ \tau_{xy} \\ \tau_{xz} \end{bmatrix} = \begin{bmatrix} E & 0 & 0 \\ 0 & k_s G & 0 \\ 0 & 0 & k_s G \end{bmatrix} \begin{bmatrix} \epsilon_{xx} \\ \gamma_{xy} \\ \gamma_{xz} \end{bmatrix} . \tag{7}$$

where E is the elasticity modulus, k_s is the shearing factor and G is the shear modulus. The complete strain tensor is obtained through

$$\mathbf{E} = \frac{1}{2} \left[\left(\frac{d\mathbf{p}}{d\mathbf{X}} \right) + \left(\frac{d\mathbf{p}}{d\mathbf{X}} \right)^T + \left(\frac{d\mathbf{p}}{d\mathbf{X}} \right)^T \left(\frac{d\mathbf{p}}{d\mathbf{X}} \right) \right] , \tag{8}$$

where $\epsilon_{xx} = \mathbf{E}_{11}$, $\gamma_{xy} = \mathbf{E}_{21}$, $\gamma_{xz} = \mathbf{E}_{31}$. The position in the non-deformed configuration is $\mathbf{X} = (x \; y \; z)^T$ and the displacement field $\mathbf{p} = (u_x \; u_y \; u_z)^T$, written in the non-deformed configuration, is such that

$$\begin{aligned} u_x &= u - y\theta_z + z\theta_y \,, \\ u_y &= v + y(\cos(\theta_x) - 1) - z\sin(\theta_x) \,, \\ u_z &= w + z(\cos(\theta_x) - 1) + y\sin(\theta_x) \,. \end{aligned} \tag{9}$$

The discretization of the linear terms yields the stiffness matrix $\mathbf{K}$ and the discretization of the higher-order terms yields the nonlinear force vector $\mathbf{f}^{se}$ that couples axial, torsional and lateral vibrations. In fact, the dynamics takes places about a prestressed configuration (see section 4.) and the geometric stiffness matrix $\mathbf{K}^g(\mathbf{u}^s)$ is used, where $\mathbf{u}^s$ is the prestressed state. There is no simplification, all the terms obtained from the strain energy are used in the formulation.

The stiffness element matrix is written as:

$$\begin{aligned} \mathbf{K}^e = \int_0^1 \Bigg[& \frac{EA}{l^e} \left(\mathbf{N}_u'^T \mathbf{N}_u' \right) + \frac{k_s G I_p}{l^e} \left(\mathbf{N}_{\theta_x}'^T \mathbf{N}_{\theta_x}' \right) + \frac{EI}{l^e} \Big(\mathbf{N}_{\theta_y}'^T \mathbf{N}_{\theta_y}' + \\ & + \mathbf{N}_{\theta_z}'^T \mathbf{N}_{\theta_z}' \Big) + \frac{k_s GA}{l^e} \left(\mathbf{N}_v'^T \mathbf{N}_v' + \mathbf{N}_w'^T \mathbf{N}_w' \right) + k_s GA l^e \Big(\mathbf{N}_{\theta_y}^T \mathbf{N}_{\theta_y} + \\ & + \mathbf{N}_{\theta_z}^T \mathbf{N}_{\theta_z} \Big) + k_s GA \Big(\mathbf{N}_v'^T \mathbf{N}_{\theta_z} + \mathbf{N}_{\theta_z}^T \mathbf{N}_v' + \mathbf{N}_w'^T \mathbf{N}_{\theta_y} + \mathbf{N}_{\theta_y}^T \mathbf{N}_w' \Big) \Bigg] d\xi \,. \end{aligned} \tag{10}$$

where the spatial derivative is denoted by $(')$ and the element displacement spatial derivatives are written as $(u^e)' = \frac{1}{l^e}\mathbf{N}'_u\mathbf{u}^e$, $(v^e)' = \frac{1}{l^e}\mathbf{N}'_v\mathbf{u}^e$, $(w^e)' = \frac{1}{l^e}\mathbf{N}'_w\mathbf{u}^e$, $({\theta_x}^e)' = \frac{1}{l^e}\mathbf{N}'_{\theta_x}\mathbf{u}^e$, $({\theta_y}^e)' = \frac{1}{l^e}\mathbf{N}'_{\theta_y}\mathbf{u}^e$, $({\theta_z}^e)' = \frac{1}{l^e}\mathbf{N}'_{\theta_z}\mathbf{u}^e$. The geometric stiffness element matrix, when the only nonzero displacement is the axial one ($\mathbf{u}^s$), may be written as

$$
\begin{aligned}
(\mathbf{K}^g(\mathbf{u}^s))^{(e)} &= (u^e)' \int_0^1 \left[\frac{AE}{(l^e)^2} \left(\mathbf{N}_v'^T\mathbf{N}'_v + \mathbf{N}_w'^T\mathbf{N}'_w + 3\mathbf{N}_u'^T\mathbf{N}'_u \right) + \right. \\
&+ \frac{k_s GA}{l^e} \left(\mathbf{N}_v'^T\mathbf{N}_{\theta_z} + \mathbf{N}_w'^T\mathbf{N}_{\theta_y} + \mathbf{N}_{\theta_z}^T\mathbf{N}'_v + \mathbf{N}_{\theta_y}^T\mathbf{N}'_w + 2l^e\mathbf{N}_{\theta_z}^T\mathbf{N}_{\theta_z} + \right. \\
&\left. \left. + 2l^e\mathbf{N}_{\theta_y}^T\mathbf{N}_{\theta_y} \right) + \frac{EI}{(l^e)^2} \left(2\mathbf{N}_{\theta_x}'^T\mathbf{N}'_{\theta_x} + 3\mathbf{N}_{\theta_y}'^T\mathbf{N}'_{\theta_y} + 3\mathbf{N}_{\theta_z}'^T\mathbf{N}'_{\theta_z} \right) \right] l^e d\xi + \\
&+ (u^e)'^2 \int_0^1 \left[k_s GA \left(\mathbf{N}_{\theta_y}^T\mathbf{N}_{\theta_y} + \mathbf{N}_{\theta_z}^T\mathbf{N}_{\theta_z} \right) + \frac{EI}{(l^e)^2} \left(\mathbf{N}_{\theta_x}'^T\mathbf{N}'_{\theta_x} + \frac{3}{2}\mathbf{N}_{\theta_y}'^T\mathbf{N}'_{\theta_y} \right. \right. \\
&\left. \left. + \frac{3}{2}\mathbf{N}_{\theta_z}'^T\mathbf{N}'_{\theta_z} \right) + \frac{EA}{(l^e)^2} \left(\frac{3}{2}\mathbf{N}_u'^T\mathbf{N}'_u + \frac{1}{2}\mathbf{N}_v'^T\mathbf{N}'_v + \frac{1}{2}\mathbf{N}_w'^T\mathbf{N}'_w \right) \right] l^e d\xi \, .
\end{aligned}
\tag{11}
$$

The nonlinear force element vector due to the strain energy is written as:

$$
\begin{aligned}
(\mathbf{f}^{se})^{(e)} &= \int_0^1 \left[\mathbf{N}_u'^T f_1 + \mathbf{N}_v^T f_2 + \mathbf{N}_w'^T f_3 + \mathbf{N}_{\theta_x}'^T f_4 + \mathbf{N}_{\theta_y}'^T f_5 + \right. \\
&\left. + \mathbf{N}_{\theta_z}'^T f_6 + \mathbf{N}_{\theta_x}^T f_7 + \mathbf{N}_{\theta_y}^T f_8 + \mathbf{N}_{\theta_z}^T f_9 \right] l^e d\xi \, ,
\end{aligned}
\tag{12}
$$

where $f_1, .., f_9$ are found in appendix B.

2.3 Impact, rubbing and stabilizers

The drill-string may impact the borehole. If the radial displacement $r = \sqrt{v^2 + w^2}$ is big enough to exceed the diameter of the borehole, there is a reaction force. This means that there is impact and rubbing if $r > (R_b - R_o)$, where R_b is the radius of the borehole and R_o is the outer radius of the column, see Fig. 3.

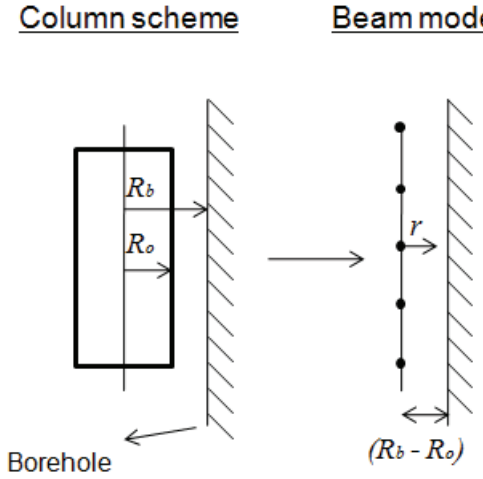

Figure 3: Scheme of the radial displacement.

The impact is modeled as an elastic force

$$
\begin{aligned}
{F_y}^{ip} &= -\mathbb{1}^{ip}(r)\; k^{ip}(r-(R_b-R_o))\frac{v}{r}\,,\\
{F_z}^{ip} &= -\mathbb{1}^{ip}(r)\; k^{ip}(r-(R_b-R_o))\frac{w}{r}\,,
\end{aligned}
\tag{13}
$$

where k^{ip} is the stiffness parameter of the impact and $\mathbb{1}^{ip}(r)$ is an indicator that is equal to one if $r > (R_b - R_o)$ and is equal to zero otherwise. Rubbing between the column and the borehole is modeled as a frictional torque

$$
{T_x}^{ip} = -\mathbb{1}^{ip}(r)\; \mu^{ip} F_n R_o\, sign(\dot{\theta}_x)\,, \tag{14}
$$

where $F_n = \sqrt{({F_y}^{ip})^2 + ({F_z}^{ip})^2}$, μ^{ip} is the friction coefficient and $sign(a)$ returns the sign of a ($sign(a) = 1$ if $a \geq 0$ and $sign(a) = -1$ if $a < 0$).

Stabilizers are used in the BHA region to make the system stiffer, thus diminishing the amplitude of the lateral vibrations. Stabilizers are modeled as an elastic element:

$$
F_y|_{x=x^{stab}} = k^{stab}\; v|_{x=x^{stab}} \quad \text{and} \quad F_z|_{x=x^{stab}} = k^{stab}\; w|_{x=x^{stab}}\;, \tag{15}
$$

where k^{stab} is the stiffness parameter of the stabilizer and x^{stab} is the location of the stabilizer.

2.4 Bit-rock interaction

For the bit-rock interaction, the model used is the one developed in Tucker and Wang (2003) because it describes well how the bit penetrates the rock. The force and torque acting at the bit may be written as

$$
\begin{aligned}
f_x^{bit} &= -\frac{\dot{u}^{bit}}{a_2 Z(\dot{\theta}^{bit})^2} + \frac{a_3\dot{\theta}^{bit}}{a_2 Z(\dot{\theta}^{bit})} - \frac{a_1}{a_2}\,,\\
t_x^{bit} &= -\frac{\dot{u}^{bit} a_4 Z(\dot{\theta}^{bit})^2}{\dot{\theta}^{bit}} - a_5 Z(\dot{\theta}^{bit})\,,
\end{aligned}
\tag{16}
$$

where f_x^{bit} is the axial force (also called weight-on-bit), t_x^{bit} is the torque about the x-axis, $a_1, \ldots, a_5$ are positive constants that depend on the bit and rock characteristics and $Z(\dot{\theta}^{bit})$ is the regularization function:

$$
Z(\dot{\theta}^{bit}) = \frac{\dot{\theta}^{bit}}{\sqrt{\left(\dot{\theta}^{bit}\right)^2 + e^2}}\,, \tag{17}
$$

where e is the regularization parameter. The regularization function and the torque in function of $\dot{\theta}^{bit}$ are plotted in Fig. 4.

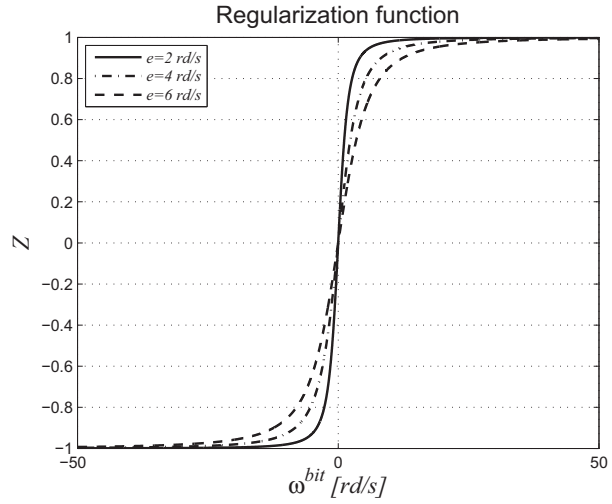

(a)

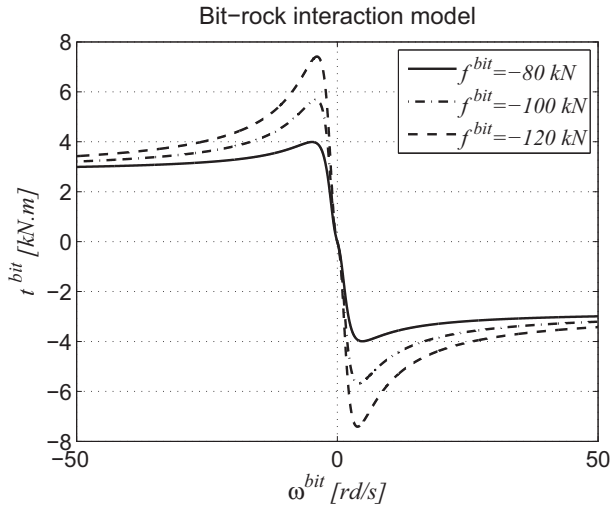

(b)

Figure 4: (a) Regularization function. (b) torque in function of $\dot{\theta}^{bit}$.

In the next section the fluid-structure interaction model is presented.

3. FLUID-STRUCTURE INTERECTION

A linear fluid-structure coupling model similar to Paidoussis (1998); Paidoussis et al. (2008) is used. The proposed simplified model assumes that the pressure varies linearly with x and that the inside flow is inviscid, while the outside flow is viscous. The flow induced by the rotation about the x-axis is not considered in the analysis. Following the strategy presented in Paidoussis et al. (2008) and extending the analysis for a 3D problem, we first write the fluid forces in x direction, highlighting the forces due to the internal and external flow:

$$F_x^f = \underbrace{M^f g - A_i \frac{\partial p_i}{\partial x}}_{internal flow} \underbrace{-F^L + \frac{\partial}{\partial x}(A_o p_o) - A_o \frac{\partial p_o}{\partial x}}_{external flow}, \tag{18}$$

where M^f is the mass per unit length, g is the gravity acceleration, A_i and A_o are the cross-sectional areas corresponding to the inner and outer diameters of the column (see Fig. 5), ρ^f is the fluid density, p_i and p_o are the inside and outside pressures and F_L is a frictional viscous force.

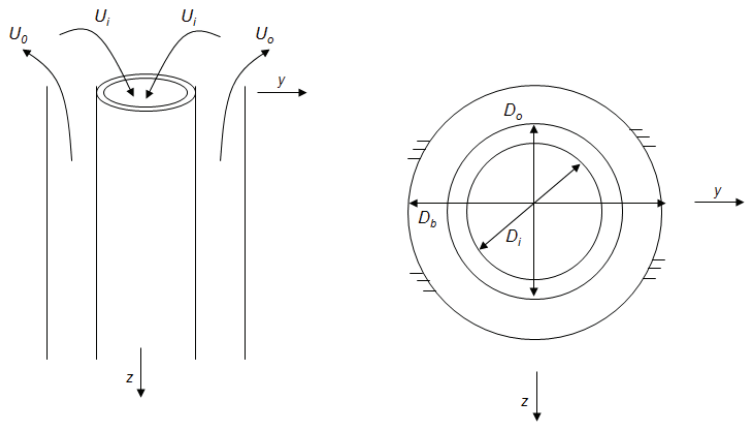

Figure 5: Scheme showing the diameters (inside, outside, borehole) and the inlet and outlet flow.

The fluid forces in z direction are written as:

$$F_z^f = \underbrace{M^f\left(\frac{\partial^2 w}{\partial t^2} + 2U_i\frac{\partial^2 w}{\partial x \partial t} + U_i^2\frac{\partial^2 w}{\partial x^2}\right) + A_i\frac{\partial}{\partial x}\left(p_i\frac{\partial w}{\partial x}\right)}_{internal\,flow} +$$

$$+\underbrace{\chi\left(\frac{\partial}{\partial t} - U_o\frac{\partial}{\partial x}\right)\left[\rho^f A_o\left(\frac{\partial w}{\partial t} - U_o\frac{\partial w}{\partial x}\right)\right] - A_o\frac{\partial}{\partial x}\left(p_o\frac{\partial w}{\partial x}\right) + F_z^N + F^L\frac{\partial w}{\partial x}}_{external\,flow}, \quad (19)$$

where U_i and U_o are the flow speed inside and outside the column, $\chi = \frac{(D_b/D_o)^2+1}{(D_b/D_o)^2-1}$ which is always > 1 and F_{Nz} is a frictional viscous force. The expressions of the frictional viscous forces are shown below:

$$F^L = \frac{1}{2}C^f\rho^f D_o U_o^2\,, \quad (20)$$

$$F_z^N = \frac{1}{2}C^f\rho^f D_o U_o\left(\frac{\partial w}{\partial t} - U_o\frac{\partial w}{\partial x}\right) + k\frac{\partial w}{\partial t}\,, \quad (21)$$

where C^f, k are the viscous damping coefficients and D_h is the hydraulic diameter $\left(D_h = \frac{4A_b}{\pi D_b + \pi D_o}\right)$. The fluid forces in y direction are similar to the ones just presented.

The pressures vary linearly with x and are written as

$$p_i = \left(\rho^f g\right)x + p^{cte}\,, \quad (22)$$

$$p_o = \left(\rho^f g + \frac{F^L}{A_o}\frac{D_o}{D_h}\right)x\,, \quad (23)$$

where p^{cte} is the pump pressure. Another assumption is that there is no head loss when the fluid passes from the drill-pipe to the drill-collar (and vice-versa). The head loss due to the change in velocity of the fluid at the bottom (it was going down, then it goes up) is given by

$$h = \frac{1}{2g}(U_i - U_o)^2 \,. \tag{24}$$

After discretization by means of the Finite Element Method, the fluid mass element matrix is written as

$$(\mathbf{M}^f)^{(e)} = \int_0^1 \left(M^f + \chi\rho^f A_o\right)(\mathbf{N}_w^T\mathbf{N}_w + \mathbf{N}_v^T\mathbf{N}_v) l^e d\xi \,, \tag{25}$$

The fluid mass matrix is the usual added mass. The fluid stiffness element matrix is written as

$$\begin{aligned}(\mathbf{K}^f)^{(e)} = &\int_0^1 \left(-M^f U_i^2 - A_i p_i + A_o p_o - \chi\rho^f A_o U_o^2\right)(\mathbf{N}_w'^T\mathbf{N}_w' + \mathbf{N}_v'^T\mathbf{N}_v')\frac{1}{l^e}d\xi + \\ &+ \int_0^1 \left(-A_i\frac{\partial p_i}{\partial x} + A_o\frac{\partial p_o}{\partial x}\right)(\mathbf{N}_{\theta_y}^T\mathbf{N}_{\theta_y} + \mathbf{N}_{\theta_z}^T\mathbf{N}_{\theta_z}) l^e d\xi \,.\end{aligned} \tag{26}$$

The fluid stiffness matrix depends on the speed of the inside and outside flow, on the pressure and on the pressure derivatives. The fluid damping element matrix is written as

$$\begin{aligned}(\mathbf{C}^f)^{(e)} = &\int_0^1 \left(-2M^f U_i + 2\chi\rho^f A_o U_o\right)(\mathbf{N}_{\theta_y}^T\mathbf{N}_{\theta_y} + \mathbf{N}_{\theta_z}^T\mathbf{N}_{\theta_z}) l^e d\xi + \\ &+ \int_0^1 \left(\frac{1}{2}C^f\rho^f D_o U_o + k\right)(\mathbf{N}_w^T\mathbf{N}_w + \mathbf{N}_v^T\mathbf{N}_v) l^e d\xi \,.\end{aligned} \tag{27}$$

The fluid damping matrix depends on the flow speed as well as on the viscous parameters of the fluid which are not well established values. There are uncertainties in the determination of the damping characteristics, but a detailed analysis will not be addressed. The axial fluid element force is written as

$$(\mathbf{f}^f)^{(e)} = \int_0^1 \left(M^f g - A_i\frac{\partial p_i}{\partial x} - \frac{1}{2}C^f\rho^f D_o U_o^2\right)\mathbf{N}_u^T l^e d\xi \,. \tag{28}$$

This force represents the buoyancy induced by the fluid. In section 5. we investigate how the dynamical characteristics of the system change with the inclusion of the fluid-structure interaction model.

4. DISCRETIZED SYSTEM OF EQUATIONS

Suppose that the column is put down in the borehole until it reaches the soil. At this point the forces acting are: the reaction force at the bit ($\mathbf{f}^c$), the weight of the drill-string ($\mathbf{f}^g$), the weight-on-hook (supporting force at the top) and the buoyancy force ($\mathbf{f}^f$). In this static equilibrium configuration we have

$$\mathbf{u}^s = \mathbf{K}^{-1}(\mathbf{f}^g + \mathbf{f}^c + \mathbf{f}^f)\,. \tag{29}$$

The vibration takes places about this configuration: $\bar{\mathbf{u}} = \mathbf{u} - \mathbf{u}^s$. The final discretized system of equations are written as

$$\begin{gathered}(\mathbf{M} + \mathbf{M}^f)\ddot{\bar{\mathbf{u}}}(t) + (\mathbf{C} + \mathbf{C}^f)\dot{\bar{\mathbf{u}}}(t) + (\mathbf{K} + \mathbf{K}^f + \mathbf{K}^g(\mathbf{u}^s))\bar{\mathbf{u}}(t) = \mathbf{f}^{NL}(t, \bar{\mathbf{u}}, \dot{\bar{\mathbf{u}}}, \ddot{\bar{\mathbf{u}}})\,, \\ \bar{\mathbf{u}}(0) = \bar{\mathbf{u}}_0 \quad , \quad \dot{\bar{\mathbf{u}}}(0) = \dot{\bar{\mathbf{u}}}_0\,,\end{gathered} \tag{30}$$

where $\bar{\mathbf{u}}_0$ and $\dot{\bar{\mathbf{u}}}_0$ are the initial conditions. It is easy to identify in Eq. (30) the mass, the stiffness and the damping matrix of the column $(\mathbf{M}, \mathbf{K}, \mathbf{C})$ and of the fluid $(\mathbf{M}^f, \mathbf{K}^f, \mathbf{C}^f)$. $\mathbf{K}^g(\mathbf{u}^s)$ is the geometric stiffness matrix and $\mathbf{f}^{NL}$ is the nonlinear force vector:

$$\mathbf{f}^{NL}(t, \bar{\mathbf{u}}, \dot{\bar{\mathbf{u}}}, \ddot{\bar{\mathbf{u}}}) = \mathbf{f}^{ke}(\bar{\mathbf{u}}, \dot{\bar{\mathbf{u}}}, \ddot{\bar{\mathbf{u}}}) + \mathbf{f}^{se}(\bar{\mathbf{u}}) + \mathbf{f}^{ip}(\bar{\mathbf{u}}) + \mathbf{f}^{bit}(\dot{\bar{\mathbf{u}}}) + \mathbf{g}(t)\,, \tag{31}$$

where $\mathbf{f}^{ke}$ and $\mathbf{f}^{se}$ are the higher-order terms obtained from the kinetic and strain energies (Eqs. (5) and (12)), $\mathbf{f}^{ip}$ and $\mathbf{f}^{bit}$ are the impact and bit-rock interaction forces (Eqs. (13), (14) and (16)), and $\mathbf{g}$ is the force that corresponds to the Dirichlet boundary condition (rotation imposed at the top).

5. NUMERICAL RESULTS

In this section, the influence of the fluid on the drill-string dynamics is investigated using a numerical example. The data used in the simulations correspond to a representative drill-string with 1600 meters length (see the data used in appendix C).

5.1 Modal analysis

The elastic modes of the structure (lateral, axial and torsional) and the associated natural frequencies are analyzed for different configurations. This analysis is essential to understand how the characteristics of the system are affected by the fluid flow.

To correctly compare the normal modes and the corresponding natural frequencies of two different configurations, the matrix $\mathbf{MAC}$ (Allemang, 2003) defined by

$$\mathbf{MAC}_{ij} = \frac{< \mathbf{\Phi}_i^1, \mathbf{\Phi}_j^2 >}{||\mathbf{\Phi}_i^1||.||\mathbf{\Phi}_j^2||} \tag{32}$$

is used, where $\mathbf{\Phi}_i^1$ is the i-th mode for the first configuration, $\mathbf{\Phi}_j^2$ is the j-th mode for the second configuration, $< \cdot, \cdot >$ denotes the Euclidean inner product and $||\cdot||$ is the associated norm. Two modes $\mathbf{\Phi}_i^1$ $\mathbf{\Phi}_j^2$ are well associated if $\mathbf{MAC}_{ij}$ has value close to one and they are not well associated if this value is close to zero.

First, the influence of the prestressed configuration is analyzed and no fluid is considered yet. Table 1 shows the natural frequencies associated with the first 10 lateral modes of the system with and without the prestressed configuration. For short, we call them lateral natural frequencies and it is implicit that they are the natural frequencies associated with the lateral modes.

Rank of the eigenvalue (prestressed config.)	1-2	3-4	5-6	7-8	9-10
prestressed (Hz)	0.0287	0.0464	0.0928	0.1098	0.1394
no prestress (Hz)	0.0127	0.0004	0.0010	0.0490	0.0020
difference (%)	55.7	99.1	98.9	55.4	98.6

Table 1: Lateral natural frequencies with and without the prestressed configuration (no fluid).

The lateral natural frequencies appear in pairs due to the symmetry about the x-axis. The first and the second normal modes have the same shape (due to the symmetry). The values of the natural frequencies change completely (with differences greater than 50%) when the prestressed state is considered. The first lateral shape for the model considering the prestressed state is associated with the ninth lateral shape for the model without the prestressed state, the second one is associated with the first one, the third one is associated with the second one, the forth is associated with the eighteenth one and so on. Sometimes the shapes are well related ($\mathbf{MAC}_{ij} \sim 1$) and sometimes the relation is not so good ($\mathbf{MAC}_{ij} < 0.5$).

Tables 2 and 3 show the differences of the axial and torsional natural frequencies comparing the column with and without the prestressed configuration.

Rank of the axial eigenvalue (prestressed config.)	1	2	3	4	5
prestressed (Hz)	1.202	2.882	4.676	6.503	8.343
no prestress (Hz)	1.201	2.879	4.672	6.496	8.336
difference (%)	0.092	0.094	0.094	0.095	0.095

Table 2: Axial natural frequencies with and without the prestressed configuration (no fluid).

Rank of the torsional eigenvalue (prestressed config.)	1	2	3	4	5
prestressed (Hz)	0.2144	1.1105	2.1526	3.2138	4.2850
no prestress (Hz)	0.2141	1.1094	2.1505	3.2107	4.2809
difference (%)	0.1401	0.0992	0.0977	0.0966	0.0958

Table 3: Torsional natural frequencies with and without the prestressed configuration (no fluid).

The axial and torsional natural frequencies are little affected by the prestressed configuration. The modes have to be well associated for the comparison, but they are always well related ($\mathbf{MAC}_{ij} \sim 1$).

Now the influence of the fluid is analyzed, always using the prestressed configuration. It should be remarked that the inclusion of the fluid does not change the axial and torsional natural frequencies of the system as it can be checked from Eqs. (25), (26) and (27).

Fig. 6 shows the comparison of the mode shapes for the model with and without the fluid.

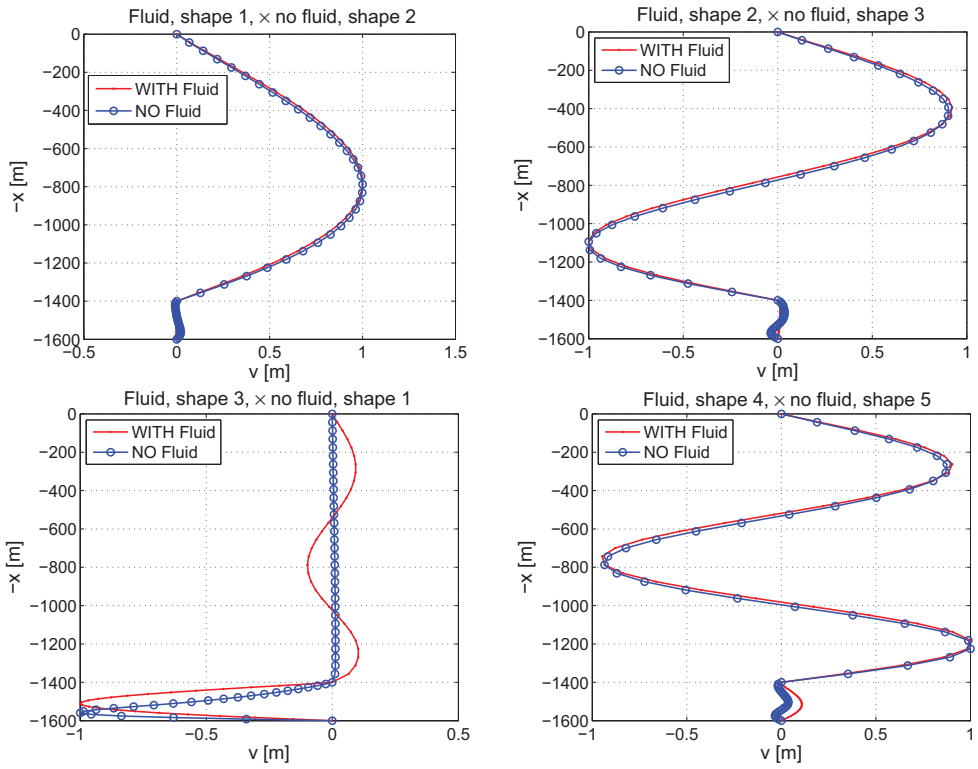

Figure 6: Comparison of the lateral modes for the model with and without fluid.

As shown in Fig. 6, the first lateral shape for the model with fluid is associated with the second lateral shape for the model without fluid, the second one is associated with the third one, the third one is associated with the first one, the fourth one is associated with the fifth one and so on. Table 4 shows a comparison of the lateral natural frequencies:

Rank of the eigenvalue (config. with fluid)	1-2	3-4	5-6	7-8	9-10
with fluid (Hz)	0.037	0.074	0.107	0.112	0.145
no fluid (Hz)	0.046	0.093	0.029	0.139	0.186
difference (%)	-24.7	-24.7	73.1	-24.8	-24.8

Table 4: Lateral natural frequencies for the model with and without the fluid.

There is a significative change in the lateral frequencies due to the presence of the fluid. Investigating the influence of each term of the fluid equations, it was found that the term $(-p_i A_i + p_o A_o)$ of the fluid stiffness matrix has a major influence on the stiffness of the system. Note that $p_i \sim p_o$ for a given depth, but in the lower region (BHA) $A_o \sim 10A_i$, which makes the system much stiffer in the bottom. Table 4 shows that the lateral natural frequencies for the model with fluid might be lower or greater than the lateral natural frequencies for the model without fluid when comparing with respect to the associated modes.

Next, it will be investigated the influence of the added mass and added stiffness separately. The influence of the damping depends on the viscous property of the fluid, but it is not analyzed in details in this paper. Table 5 shows the differences of the lateral natural frequencies for the added mass only and for the added stiffness only.

Rank of the eigenvalue (config. without fluid)	1-2	3-4	5-6	7-8	9-10
no fluid (Hz)	0.029	0.046	0.093	0.110	0.140
added mass only (Hz)	0.023	0.036	0.072	0.087	0.108
difference (%)	-20.7	-22.8	-22.8	-20.7	-22.8
no fluid (Hz)	0.029	0.046	0.093	0.110	0.140
added stiffness only (Hz)	0.134	0.048	0.096	0.273	0.145
difference (%)	367.9	3.7	3.8	148.2	3.7

Table 5: Influence of the added fluid mass and stiffness on the lateral frequencies.

The presence of the fluid adds around 50% of mass, this is why the natural frequencies are around 20% lower. It should be noted that the shapes of the lateral modes practically do not change when only the fluid mass is considered. The changes in the mode shapes occur mainly due to the fluid added stiffness. The first lateral shape for the model without fluid is associated with the third lateral shape for the model with added fluid stiffness, the second one is associated with the first one, the third one is associated with the second one, the fourth one is associated with the seventh one and so on.

Now, the influence of the inside and outside flow are investigated separately. Table 6 shows the differences of the lateral natural frequencies for the inside flow only and for the outside flow only.

Rank of the eigenvalue (config. without fluid)	1-2	3-4	5-6	7-8	9-10
no fluid (Hz)	0.029	0.046	0.093	0.110	0.140
inside flow (Hz)	$0.080\sqrt{-1}$	0.040	0.080	0.064	0.121
difference (%)	-	-13.6	-13.4	-42.0	-13.5
no fluid (Hz)	0.029	0.046	0.093	0.110	0.140
outside flow (Hz)	0.113	0.041	0.082	0.228	0.124
difference (%)	292.3	-11.2	-11.2	107.7	-11.3

Table 6: Influence of the added fluid mass and stiffness on the lateral frequencies.

The inside flow makes the system less stiff and unstable: the first eigenvalue is imaginary, indicating that the system is unstable. The outside flow increases the eigenfrequencies associated with some lateral modes and decreases others.

Finally, Table 7 shows the difference in the lateral natural frequencies when the flow speed is increased. It is noted that the flow speed is not so important to change significantly the dynamic characteristics of the structure.

Rank of the eigenvalue	1-2	3-4	5-6	7-8	9-10
U_i=1.5 m s^{-1} (Hz)	0.0372	0.0744	0.1065	0.1117	0.1488
U_i=10 m s^{-1} (Hz)	0.0368	0.0736	0.1066	0.1106	0.1473
difference (%)	1.0753	1.0753	-0.0939	0.9848	1.0081

Table 7: Influence of the flow on the lateral frequencies.

5.2 Dynamical response

The column was discretized with 56 finite elements. For the time integration, the Newmark scheme was used together with an iteration method (fixed point) to solve the nonlinear algebraic

Eq. (30) at each time step ($\Delta t = 5 \times 10^{-5}$).

As initial conditions, all the points of the column have a given axial speed $\dot{u}_0$ (4.2×10^{-3} m s^{-1}), a given rotational speed about the x-axis ω_{x0} (5.236 rd s^{-1}) and a given lateral displacement.

Fig. 7 shows the radial response ($r = \sqrt{v^2 + w^2}$) at two points: $x = 700$ m and $x = 1520$ m. Fig. 7(a) shows the dynamical response of the middle point of the drill-pipe region (the upper part) which is the point that presents the maximum radial displacement. The amplitude of the displacement begins small and then it increases until a certain value. The opposite happens for the radial displacement in the BHA region (the bottom part): the amplitude of the displacement decreases until a certain value, see Fig. 7(b). There is an exchange of energy between the modes, then the radial displacement gets bigger in the less stiff region (the drill-pipe region). If the nonlinearities that come from the kinetic and strain energies were neglected ($\mathbf{f}_{se} = \mathbf{f}_{ke} = 0$), the amplitude of the lateral displacement would vanish because there would be no coupling between the lateral vibration and the axial and the torsional ones. All of these effects happen due to the vibration coupling induced by these nonlinearities.

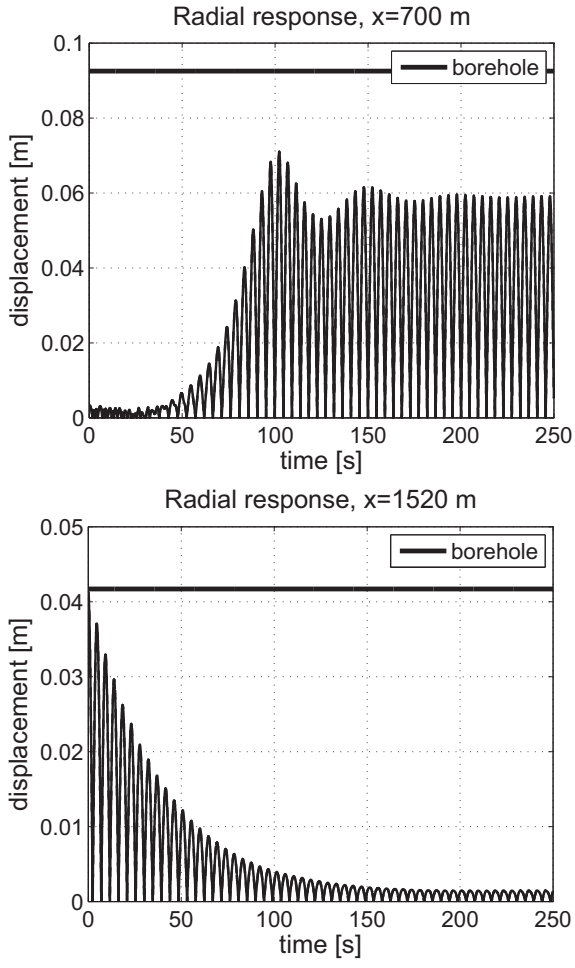

Figure 7: Radial response at $x = 700$ m (a) and $x = 1520$ m (b). Note that the distance between the column and the borehole is different depending on the region of the column considered.

For the next analysis the response is considered for $t > t^t$. Time t^t was identified such that after $t = t^t$ the transient part vanishes, so that for $t \in [t^t, t[$ there is only the forced response.

Fig. 8(a) shows the axial speed at $x = 700$ m and Fig. 8(b) shows its Fourier transform.

The fundamental frequency 0.220 Hz is a little bigger than the first torsional natural frequency which is 0.214 Hz. The fundamental frequency corresponds to the self-excited vibration of the system that is related to the torsional vibration imposed by the bit-rock interaction. Due to the nonlinearities of the system, the multiples $0.220 \times i$ (with $i = 1, 2, ..$) of the fundamental frequency appear in the frequency spectrum.

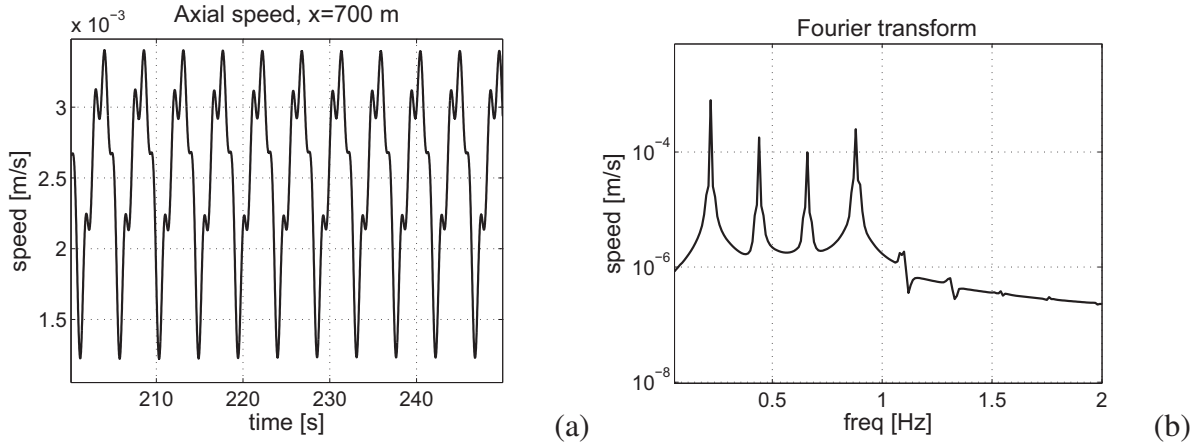

Figure 8: Response at $x = 700$ m. Axial speed (a) and its Fourier transform (b).

Fig. 9(a) shows the rotational speed about the x-axis at $x = 700$ m and Fig. 9(b) shows its Fourier transform. The bit-rock interaction acts on the axial speed and on the rotational speed about the x-axis, therefore the same kind of frequency spectrum is observed for the rotational speed about the x-axis and for the axial speed.

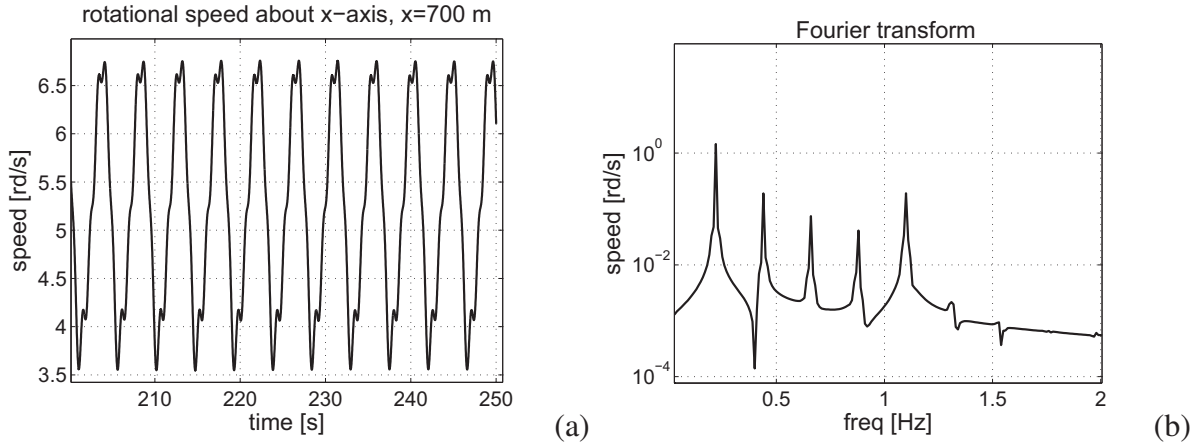

Figure 9: Response at $x = 700$ m. Rotational speed about the x-axis (a) and its Fourier transform (b).

Fig. 10(a) shows the rotation about the z-axis and Fig. 10(b) shows its Fourier transform. The dominant frequency, 0.110 Hz, is equal to the half of the fundamental frequency related to the self excited vibration. The frequency spectrum shows the multiples $0.110 \times i$ (with $i = 1, 3, 5, ..$). The same behavior is observed for the lateral response v, Figs. 11(a) and (b).

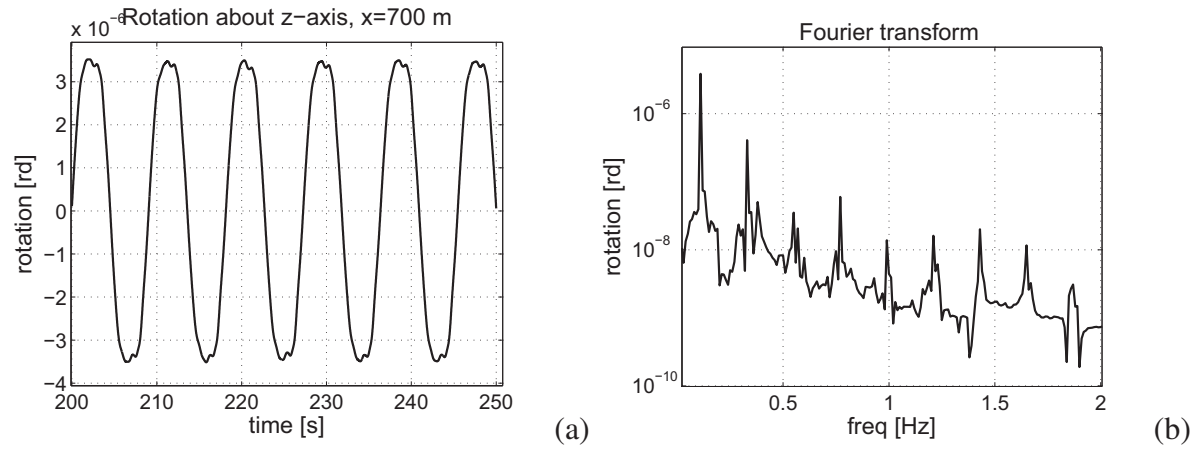

Figure 10: Response at $x = 700$ m. Rotation about the z-axis (a) and its Fourier transform (b).

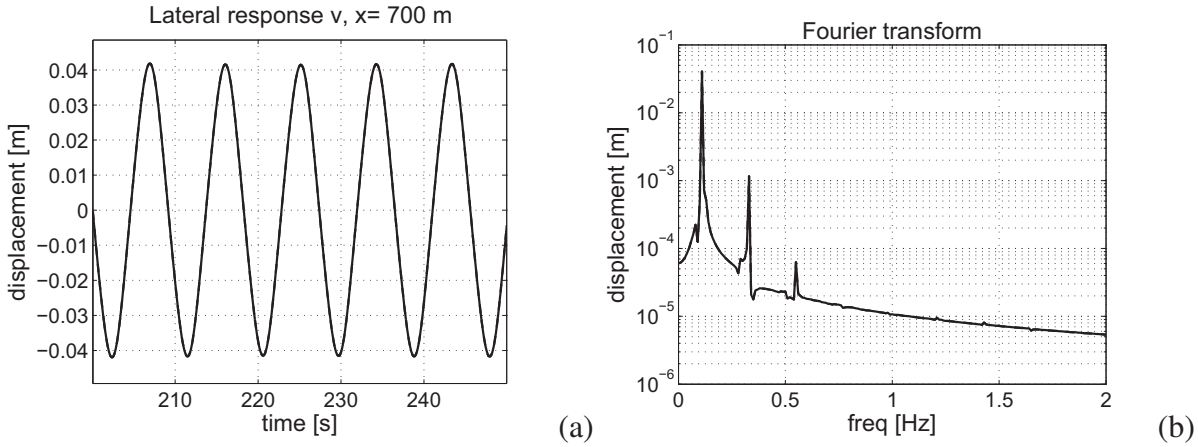

Figure 11: Response at $x = 700$ m. Lateral displacement v (a) and its Fourier transform (b).

Next, the dynamical response for the model with and without the fluid are compared. Fig. 12 shows the radial response for $t = [0, 250]$s at $x = 1560$ m. To better compare the two dynamical responses, the forced response is analyzed.

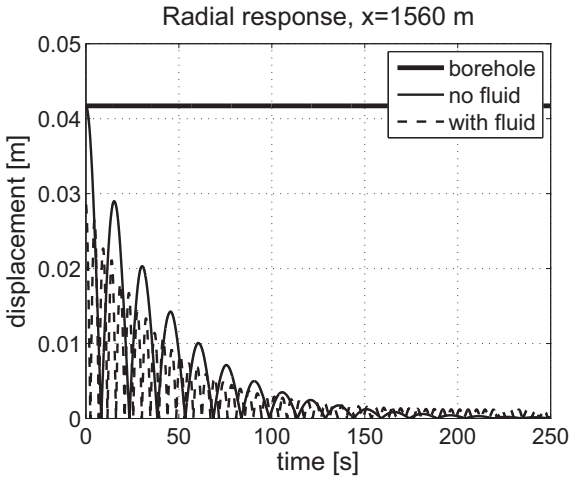

Figure 12: Comparison of the dynamical response for model with and without fluid. Radial response at $x = 1560$ m.

Fig. 13 shows the forced response of the radial displacement at $x = 700$m. The displacement is shown in log-scale. The radial response is bigger when the fluid is considered in the model. This might be explained by the shape of the first lateral modes: when the fluid is considered, the upper region is more flexible than the bottom region (see the mode shapes in Fig. 6), so the amplitude of vibration gets bigger in the upper region. It can be observed in Fig. 13 that the self excited frequency is dominating the movement of both dynamics.

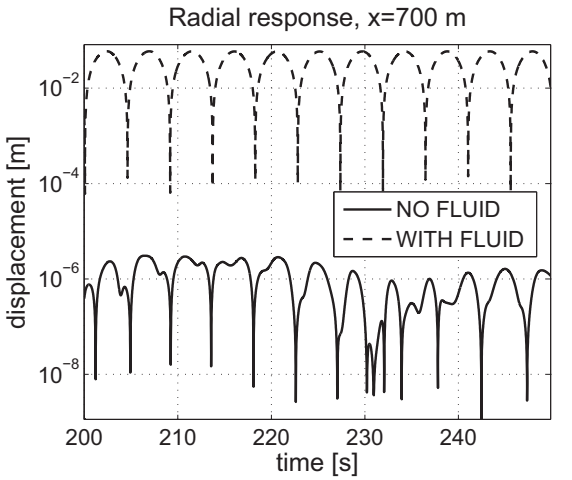

Figure 13: Comparison of the dynamical response for model with and without fluid. Radial response at $x = 700$ m.

The axial and torsional vibrations are also affected by the presence of the fluid: the fundamental (self excited) frequency changes when the fluid is taken into account. Fig. 14(a) and (b) shows the axial speed of the bit (or rate-of-penetration) and its Fourier transform. When the fluid is not taken into account, the fundamental frequency 0.210 Hz is a little lower than the first torsional natural frequency which is 0.214 Hz.

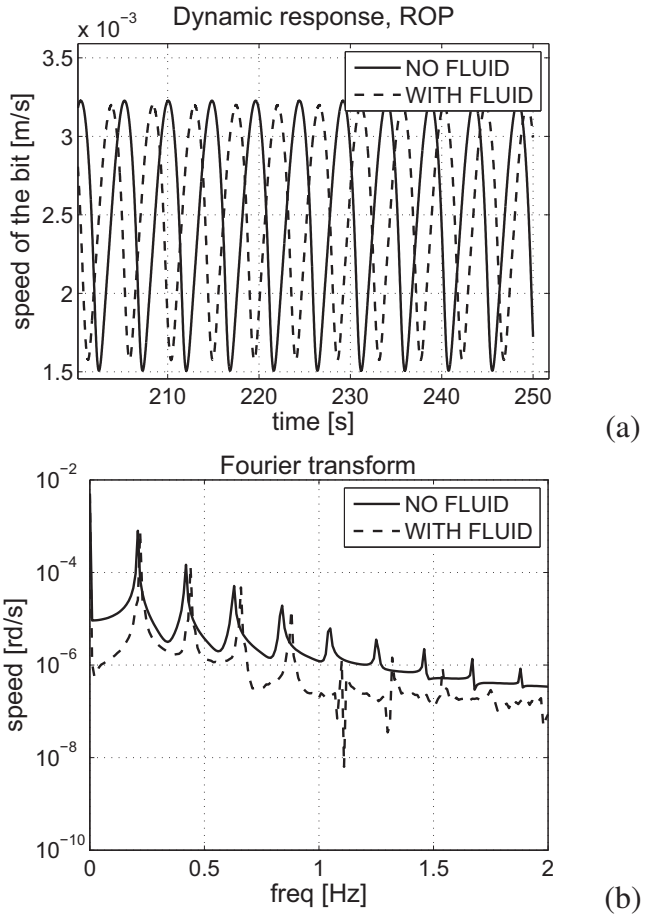

Figure 14: Comparison of the dynamical response for model with and without fluid. Rate-of-penetration (ROP) (a) and its Fourier transform (b).

6. CONCLUSIONS

The drill-string dynamics accounting for the drilling fluid (mud) has been analyzed in this paper. Note that the large majority of the published papers dealing with the nonlinear dynamics of a drill-string does not consider the fluid-structure interaction. The column has been modeled using the Timoshenko beam theory and discretized by means of the Finite Element Method. Finite strains (which couple axial, lateral and torsional vibrations) are considered with no simplifications and the dynamics is calculated in a prestressed configuration. A bit-rock interaction model that describes how the bit penetrates the soil is used and impact and rubbing between the column and the borehole are taken into account.

The fluid-structure interaction model found in Paidoussis et al. (2008) has been extended for the analyzed problem. The fluid that flows downward inside the column and then upward in the annulus is modeled in a simple way: the influence of the fluid is included in the model by adding three matrices – mass, damping and stiffness – and a force that are time–independent. It has been observed that the presence of the fluid changes the dynamical response of the system, especially the lateral vibration of the structure. The amplitude of the axial and torsional vibrations are little affected, but the self excited frequency of the system (which is related to the first torsional natural frequency) changes when the fluid is taken into account.

The added fluid damping has not been analyzed but, as there are many uncertainties involving the damping of the structure, the best strategy would be to model theses uncertainties using, for instance, the probability theory. Such approach is in progress.

A SHAPE FUNCTIONS

Linear shape functions are used for the axial and torsional displacements, and the shape functions for the lateral displacements are derived by calculating the static response of the beam (Nelson, 1980; Bazoune and Khulief, 2002):

$$\mathbf{N}_u = [(1-\xi) \quad 0 \quad 0 \quad 0 \quad 0 \quad 0 \quad \xi \quad 0 \quad 0 \quad 0 \quad 0 \quad 0]\,,$$

$$\mathbf{N}_v = [0 \quad N_{w1} \quad -N_{w2} \quad 0 \quad 0 \quad 0 \quad 0 \quad N_{w3} \quad -N_{w4} \quad 0 \quad 0 \quad 0]\,,$$

$$\mathbf{N}_w = [0 \quad 0 \quad 0 \quad N_{w1} \quad N_{w2} \quad 0 \quad 0 \quad 0 \quad 0 \quad N_{w3} \quad N_{w4} \quad 0]\,,$$

$$\mathbf{N}_{\theta_x} = [0 \quad 0 \quad 0 \quad 0 \quad 0 \quad (1-\xi) \quad 0 \quad 0 \quad 0 \quad 0 \quad 0 \quad \xi]\,,$$

$$\mathbf{N}_{\theta_y} = [0 \quad 0 \quad 0 \quad N_{\theta1} \quad N_{\theta2} \quad 0 \quad 0 \quad 0 \quad 0 \quad N_{\theta3} \quad N_{\theta4} \quad 0]\,,$$

$$\mathbf{N}_{\theta_z} = [0 \quad -N_{\theta1} \quad N_{\theta2} \quad 0 \quad 0 \quad 0 \quad 0 \quad -N_{\theta3} \quad N_{\theta4} \quad 0 \quad 0 \quad 0]\,,$$

where ξ is the element coordinate ($\xi = x/l^e$) and:

$$N_{w1} = \tfrac{1}{1+\varphi}\left(1 - 3\xi^2 + 2\xi^3 + \varphi\,(1-\xi)\right)\,,$$

$$N_{w2} = \tfrac{l^e}{1+\varphi}\left(-\xi + 2\xi^2 - \xi^3 + \tfrac{\varphi}{2}\,(\xi^2 - \xi)\right)\,,$$

$$N_{w3} = \tfrac{1}{1+\varphi}\left(3\xi^2 - 2\xi^3 + \varphi\xi\right)\,,$$

$$N_{w4} = \tfrac{l^e}{1+\varphi}\left(\xi^2 - \xi^3 + \tfrac{\varphi}{2}\,(\xi - \xi^2)\right)\,,$$

$$N_{\theta1} = \tfrac{1}{(1+\varphi)l^e}\left(6\xi - 6\xi^2\right)\,,$$

$$N_{\theta2} = \tfrac{1}{1+\varphi}\left(1 - 4\xi + 3\xi^2 + \varphi\,(1-\xi)\right)\,,$$

$$N_{\theta3} = \tfrac{1}{(1+\varphi)l^e}\left(-6\xi + 6\xi^2\right)\,,$$

$$N_{\theta4} = \tfrac{1}{1+\varphi}\left(-2\xi + 3\xi^2 + \varphi\xi\right)\,.$$

with $\varphi = \dfrac{12EI}{k_s GA(l^e)^2}$. Where E is the elasticity modulus, I is the area moment of inertia (y-z plane), k_s is shearing factor, G is the shear modulus, A is the cross-sectional area and l^e is the length of an element.

B NONLINEAR FORCES DUE TO THE STRAIN ENERGY

The nonlinear force element vector due to the strain energy is written as shown in Eq. (12):

$$(\mathbf{f}^{se})^{(e)} = \int_0^1 \Big[\mathbf{N}_u'^T f_1 + \mathbf{N}_v'^T f_2 + \mathbf{N}_w'^T f_3 + \mathbf{N}_{\theta_x}'^T f_4 + \mathbf{N}_{\theta_y}'^T f_5 +$$
$$+\mathbf{N}_{\theta_z}'^T f_6 + \mathbf{N}_{\theta_x}^T f_7 + \mathbf{N}_{\theta_y}^T f_8 + \mathbf{N}_{\theta_z}^T f_9\Big]\, l^e d\xi\,,$$

where this organization is chosen in a way that its computation is fast. $f_1, .., f_9$ are written as:

$$
\begin{aligned}
&-f_1 = k_s GA\left(((\theta_y^e)^2 + (\theta_z^e)^2)(1 + (u^e)') + \theta_y^e((w^e)'\cos(\theta_x^e) - (v^e)'\sin(\theta_x^e)) + \right.\\
&-\theta_z^e((v^e)'\cos(\theta_x^e) + (w^e)'\sin(\theta_x^e))) + EI\left((\theta_x^e)'^2(1 + (u^e)') + \right.\\
&+\frac{3}{2}(\theta_y^e)'^2(1 + (u^e)') + \frac{3}{2}(\theta_z^e)'^2(1 + (u^e)') + (\theta_x^e)'((v^e)'((\theta_z^e)'\sin(\theta_x^e) + \\
&-(\theta_y^e)'\cos(\theta_x^e)) - (w^e)'((\theta_z^e)'\cos(\theta_x^e) + (\theta_y^e)'\sin(\theta_x^e)))\Big) + \\
&+AE\left(\frac{3}{2}(u^e)'^2 + \frac{1}{2}(u^e)'^3 + \frac{1}{2}(v^e)'^2(1 + (u^e)') + \frac{1}{2}(w^e)'^2(1 + (u^e)')\right),
\end{aligned}
\tag{B1}
$$

$$
\begin{aligned}
&-f_2 = k_s GA\left(-\theta_z^e\cos(\theta_x^e)(1 + (u^e)') - \theta_y^e\sin(\theta_x^e)(1 + (u^e)')\right) + \\
&+EI\left((v^e)'(2(\theta_x^e)'^2 + \frac{1}{2}(\theta_y^e)'^2 + \frac{1}{2}(\theta_z^e)'^2) - (\theta_x^e)'(\theta_y^e)'\cos(\theta_x^e)(1 + (u^e)') + \right.\\
&+(\theta_x^e)'(\theta_z^e)'\sin(\theta_x^e)(1 + (u^e)')) + AE(v^e)'\left((u^e)' + \frac{1}{2}(u^e)'^2 + \frac{1}{2}(w^e)'^2 + \right.\\
&\left.+\frac{1}{2}(v^e)'^2\right),
\end{aligned}
\tag{B2}
$$

$$
\begin{aligned}
&-f_3 = k_s GA\left(\theta_y^e\cos(\theta_x^e)(1 + (u^e)') - \theta_z^e\sin(\theta_x^e)(1 + (u^e)')\right) + \\
&+EI\left((w^e)'(2(\theta_x^e)'^2 + \frac{1}{2}(\theta_y^e)'^2 + \frac{1}{2}(\theta_z^e)'^2) - (\theta_x^e)'(\theta_z^e)'\cos(\theta_x^e)(1 + (u^e)') + \right.\\
&-(\theta_x^e)'(\theta_y^e)'\sin(\theta_x^e)(1 + (u^e)')\Big) + AE(w^e)'\left((u^e)' + \frac{1}{2}(u^e)'^2 + \frac{1}{2}(v^e)'^2 + \right.\\
&\left.+\frac{1}{2}(w^e)'^2\right),
\end{aligned}
\tag{B3}
$$

$$
\begin{aligned}
&-f_4 = k_s GI\left(-\theta_y^e(\theta_z^e)' + \theta_z^e(\theta_y^e)'\right) + (EI_2 + EI_4)(\theta_x^e)'\left((\theta_x^e)'^2 + \frac{1}{2}(\theta_z^e)'^2 + \right.\\
&\left.+\frac{1}{2}(\theta_y^e)'^2\right) + EI\left((\theta_x^e)'(2(u^e)' + (u^e)'^2 + 2(v^e)'^2 + 2(w^e)'^2) + \right.\\
&+(v^e)'(\theta_z^e)'\sin(\theta_x^e)(1 + (u^e)') - (v^e)'(\theta_y^e)'\cos(\theta_x^e)(1 + (u^e)') + \\
&-(w^e)'(\theta_y^e)'\sin(\theta_x^e)(1 + (u^e)') - (w^e)'(\theta_z^e)'\cos(\theta_x^e)(1 + (u^e)')\Big).
\end{aligned}
$$

(B4)

At this point we should define the area moments of inertia I_2 and I_4.

$$I_2 = \int_A y^2 z^2 dA\,,$$

$$I_4 = \int_A y^4 dA = \int_A z^4 dA\,.$$

Back to the functions:

$$\begin{aligned}
-f_5 = {} & k_s GI\left((\theta_x^e)'\theta_z^e + (\theta_y^e)'(\theta_y^e)^2 + (\theta_y^e)'(\theta_z^e)^2\right) + EI_2(\theta_y^e)'\left(\frac{1}{2}(\theta_x^e)'^2 + \frac{3}{2}(\theta_z^e)'^2\right) + \\
& + EI_4(\theta_y^e)'\left(\frac{1}{2}(\theta_x^e)'^2 + \frac{1}{2}(\theta_y^e)'^2\right) + EI\left(-(v^e)'(\theta_x^e)'\cos(\theta_x^e)(1+(u^e)') + \right. \\
& \left. -(w^e)'(\theta_x^e)'\sin(\theta_x^e)(1+(u^e)') + (\theta_y^e)'(3(u^e)' + \frac{3}{2}(u^e)'^2 + \frac{1}{2}(v^e)'^2 + \frac{1}{2}(w^e)'^2)\right)\,,
\end{aligned}$$

(B5)

$$-f_6 = k_s GI\left((\theta_x^e)'\theta_y^e + (\theta_z^e)'(\theta_z^e)^2 + (\theta_z^e)'(\theta_y^e)^2\right) + EI_2(\theta_z^e)'\left(\frac{1}{2}(\theta_x^e)'^2 + \frac{3}{2}(\theta_y^e)'^2\right) +$$
$$+EI_4(\theta_z^e)'\left(\frac{1}{2}(\theta_x^e)'^2 + \frac{1}{2}(\theta_z^e)'^2\right) + EI\left(-(w^e)'(\theta_x^e)'\cos(\theta_x^e)(1+(u^e)')+\right.$$
$$\left.+(v^e)'(\theta_x^e)'\sin(\theta_x^e)(1+(u^e)') + (\theta_z^e)'(3(u^e)' + \frac{3}{2}(u^e)'^2 + \frac{1}{2}(v^e)'^2 + \frac{1}{2}(w^e)'^2)\right) ,$$

(B6)

$$-f_7 = k_s GA\left(-(w^e)'\theta_z^e\cos(\theta_x^e)(1+(u^e)') - (w^e)'\theta_y^e\sin(\theta_x^e)(1+(u^e)') +\right.$$
$$+(v^e)'\theta_z^e\sin(\theta_x^e)(1+(u^e)') - (v^e)'\theta_z^e\cos(\theta_x^e)(1+(u^e)')) +$$
$$+EI(\theta_x^e)'\left((v^e)'(\theta_z^e)'\cos(\theta_x^e)(1+(u^e)') + (v^e)'(\theta_y^e)'\sin(\theta_x^e)(1+(u^e)') +\right.$$
$$\left.-(w^e)'(\theta_y^e)'\cos(\theta_x^e)(1+(u^e)') + (w^e)'(\theta_z^e)'\sin(\theta_x^e)(1+(u^e)')\right) ,$$

(B7)

$$-f_8 = k_s GI\left(\theta_y^e(\theta_y^e)'^2 + \theta_y^e(\theta_z^e)'^2 - (\theta_z^e)'(\theta_x^e)'\right) + k_s GA\left(\theta_y^e(u^e)'(2+(u^e)') +\right.$$
$$\left.-(v^e)'\sin(\theta_x^e)(1+(u^e)') + (w^e)'\cos(\theta_x^e)(1+(u^e)')\right) ,$$

(B8)

$$-f_9 = k_s GI\left(\theta_z^e(\theta_z^e)'^2 + \theta_z^e(\theta_y^e)'^2 + (\theta_y^e)'(\theta_x^e)'\right) + k_s GA\left(\theta_z^e(u^e)'(2+(u^e)') +\right.$$
$$\left.-(w^e)'\sin(\theta_x^e)(1+(u^e)') - (v^e)'\cos(\theta_x^e)(1+(u^e)')\right) .$$

(B9)

C DATA USED IN THE SIMULATION

$\Omega_{x=0} = 5.236$ [rd s^{-1}] (imposed rotational speed about the x-axis at $x = 0$ m),
$f^c = 100$ [kN] (initial reaction force at the bit),
$L^{dp} = 1400$ [m] (length of the drill pipe),
$L^{dc} = 200$ [m] (length of the drill collar), ${D_o}^{dp} = .127$ [m] (outside diameter of the drill pipe),
${D_o}^{dc} = .2286$ [m] (outside diameter of the drill collar),
${D_i}^{dp} = .095$ [m] (inside diameter of the drill pipe),
${D_i}^{dc} = 0.0762$ [m] (inside diameter of the drill collar),
$D_b = 0.3$ [m] (diameter of the borehole),
$x^{stab} = 1400$ [m] (location of the stabilizer),
$k^{stab} = 17.5$ [MN m^{-1}] (stiffness per meter used for the stabilizer),
$E = 210$ [GPa] (elasticity modulus of the drill string material),
$\rho = 7850$ [kg m^{-3}] (density of the drill string material),

$\nu = .29$ [-] (poisson coefficient of the drill string material),
$k_s = 6/7$ [-] (shearing correcting factor),
$k^{ip} = 1e8$ [N m^{-1}] (stiffness per meter used for the impact),
$\mu^{ip} = 0.0005$ [-] (friction coefficient between the string and the borehole),
$u^{in} = 1.5$ [m s^{-1}] (inlet flow speed),
$\rho^f = 1200$ [kg m^{-3}] (density of the fluid),
$C^f = .0125$ [-] (fluid viscous damping coefficient),
$k = 0$ [-] (fluid viscous damping coefficient),
$g = 9.81$ [m s^{-2}] (gravity acceleration),
$a_1 = 3.429e - 3$ [m s^{-1}],
$a_2 = 5.672e - 8$ [m N^{-1} s^{-1})],
$a_3 = 1.374e - 4$ [m rd^{-1}],
$a_4 = 9.537e6$ [N rd],
$a_5 = 1.475e3$ [N m] (constants of the bit-rock interaction model),
$e = 2$ [rd/s] (regularization parameter). The damping matrix is constructed using the relationship $\mathbf{C} = \alpha(\mathbf{M} + \mathbf{M}^f) + \beta(\mathbf{K} + \mathbf{K}^f + \mathbf{K}^g(\mathbf{u}^s))$ with $\alpha = .0047$ and $\beta = .002$.

Acknowledgements

The author would like to thank the financial support of the Brazilian agencies CNPq, CAPES and FAPERJ.

REFERENCES

Allemang, J. R., 2003. The modal assurance criterion – twenty years of use and abuse. *Sound and Vibration*, vol. 37, n. 8, pp. 14–21.

ASME, 2005. *Handbook: Drilling fluids processing*. Elsevier, Inc., Burlington, Massachusetts.

Bazoune, A. & Khulief, Y., 2002. Shape functions of the three-dimensional Timoshenko beam element. *Journal of Sound and Vibration*, vol. 259, n. 2, pp. 473–480.

Christoforou, A. P. & Yigit, A. S., 2003. Fully coupled vibrations of actively controlled drillstrings. *Journal of Sound and Vibration*, vol. 267, pp. 1029–1045.

Coussot, P., Bertrand, F., & Herzhaft, B., 2004. Rheological behavior of drilling muds, characterization using MRI vizualization. *Oil and Gas Science and Technology*, vol. 59, n. 1, pp. 23–29.

Escudier, M. P., Gouldson, I. W., Oliveira, P. J., & Pinho, F. T., 2000. Effects of inner cylinder rotation on laminar flow of a newtonian fuid through an eccentric annulus. *International Journal of Heat and Fluid Flow*, vol. 21, pp. 92–103.

Escudier, M. P., Oliveira, P. J., & Pinho, F. T., 2002. Fully developed laminar flow of purely viscous non-newtonian liquids through annuli, including the effects of eccentricity and inner-cylinder rotation. *International Journal of Heat and Fluid Flow*, vol. 23, pp. 52–73.

Khulief, Y., Al-Sulaiman, F. A., & Bashmal, S., 2007. Vibration analysis of drillstrings with self excited stick-slip oscillations. *Journal of Sound and Vibration*, vol. 299, pp. 540–558.

Nelson, H. D., 1980. A finite rotating shaft element using Timoshenko beam theory. *Journal of Mechanical Design*, vol. 102, pp. 793–803.

Paidoussis, M. P., 1998. *Fluid-Structure Interactions: Slender structures and Axial Flow*, volume 1. Academic Press, London, United Kingdom.

Paidoussis, M. P., Luu, T. P., & Prabhakar, S., 2008. Dynamics of a long tubular cantilever conveying fluid downwards, which then flows upwards around the cantilever as a confined annular flow. *Journal of Fluids and Structures*, vol. 24, pp. 111–128.

Pina, E. P. F. & Carvalho, M. S., 2006. Three-dimensional flow of a newtonian liquid through an annular space with axially varying eccentricity. *Journal of Fluids Engineering*, vol. 128, n. 2, pp. 223–231.

Richard, T., Germay, C., & Detournay, E., 2007. A simplified model to explore the root cause of stick–slip vibrations in drilling systems with drag bits. *Journal of Sound and Vibration*, vol. 305, pp. 432–456.

Trindade, M. A., Wolter, C., & Sampaio, R., 2005. Karhunen–Loève decomposition of coupled axial/bending of beams subjected to impacts. *Journal of Sound and Vibration*, vol. 279, pp. 1015–1036.

Tucker, R. W. & Wang, C., 1999. An integrated model for drill-string dynamics. *Journal of Sound and Vibration*, vol. 224, n. 1, pp. 123–165.

Tucker, R. W. & Wang, C., 2003. Torsional vibration control and cosserat dynamics of a drill-rig assembly. *Meccanica*, vol. 38, n. 1, pp. 143–159.